*Materials Science-Poland, 37(4), 2019, pp. 590-598*
*http://www.materialsscience.pwr.wroc.pl/*
*DOI: 10.2478/msp-2019-0080*

# Study of crystallographic, optical and sensing properties of $Na_2WO_4$ films deposited by thermal evaporation with several thickness

B. ABDALLAH*, M. KAKHIA, S. ABOU SHAKER

Atomic Energy Commission, Department of Physics, P.O. Box 6091, Damascus, Syria

$Na_2WO_4$ films have been grown at 400 °C using thermal evaporation technique. Their structural properties were characterized by XRD, while their chemical composition was verified by both EDX and X-ray photoelectron spectroscopy (XPS). The evolution of crystallinity was studied as a function of film thickness that ranged from 500 nm to 3000 nm. The grain size increased with increasing film thickness. The surface morphology of the prepared films was studied using scanning electron microscope (SEM) and atomic force microscopy (AFM). It has been observed that the average transmittance of samples in the visible and near infrared range has varied from 90 % to 78 % with the film thickness. The optical band gap of the $Na_2WO_4$ films varied from 3.8 eV to 4.1 eV. The crystalline size increased with increasing thickness and showed better sensing response to gases. Thus, this study confirmed the possibility of using $Na_2WO_4$ thick films as a sensor element for detection of ethanol ($C_2H_5OH$), acetone ($C_3H_6O$) methanol ($CH_3OH$) and ammonia hydroxide ($NH_4OH$) vapor at room temperature, where thicker films exhibited sensing properties with a maximum sensitivity at 25 °C in air, especially for $NH_4OH$.

Keywords: *$Na_2WO_4$ films; thermal evaporation; sensing properties*

## 1. Introduction

The attractive properties of tungsten oxide ($WO_3$) have been observed for many years. The compound is widely used as a photocatalyst and it has visible-light photoactivity. There are many studies aiming at the development of improved processing routes for its deposition. Its photoactivity properties have been observed during oxidation of methanol and water splitting [1]. $WO_3$ has good resistance to photocorrosion and also exhibits low band gap (2.6 eV) as an oxide semiconductor. The electrical, optical and structural properties were studied for the films prepared in different conditions, which showed various states, amorphous for $H_xWO_3$ [2] and for $Na_xWO_3$ [3]. $Na_xWO_3$ films have perovskite-like structure with a cubic lattice where their thermodynamical stability and superconductivity are x dependent [4, 5]. In the previous work [6] $Na_2WO_4$ films have been prepared using ultrasonic spray pyrolysis. The films were prepared from aqueous solution containing $Na_2WO_4 \cdot 2H_2O$ at 475 °C and were characterized by XRD and SEM techniques. The chemical composition of the films was verified by EDX and PIXE and its formula $Na_2WO_4$ was confirmed by XRD. The results obtained by Dakhel et al. [7], showed that it is possible to use $Na_2WO_4$ crystals doped with magnetic ions for optoelectronic applications that reveal magnetic action.

It is known that metal oxides have efficacy in detecting various gases with good sensitivity. $WO_3$ has been used for $NO_2$ gas sensing applications usually at temperatures up to 200 °C or 500 °C [8]. The long-term stability of the metal oxide at higher operating temperatures results from diffusion of oxygen vacancies in the metal oxides [9]. $WO_3$ has been proposed for detection of different types of gases, such as ethanol [10], $H_2$ [11], $CH_3SH$ [12], $CO_2$ [13] and $O_3$ [14]. Also, because ammonia gas is dangerous, all industries should install an alarm system that monitors it.

Many deposition methods, such as chemical bath deposition (CBD) [15], pulsed laser

*E-mail: pscientific27@aec.org.sy

ablation [16], RF magnetron sputtering technique [17] and spray pyrolysis (USP) [18] have been developed to prepare $WO_3$ films. Thermal vacuum evaporation technique [19] is a physical vapor deposition process (PVD) in which the atoms or molecules from a thermal vaporization source reach the substrate without collisions with residual gas molecules in a vacuum chamber. This type of PVD process requires a vacuum better than $10^{-3}$ Pa [20], with substrates heated at high temperature of about 600 °C [21]. Rod-like structures of tungsten oxide having nanometer scale diameter were formed under appropriately chosen growth conditions [22]. Vacuum evaporation technique has been adopted in this work to deposit $Na_2WO_4$ thin films on Si and glass substrates. In order to investigate the effect of thickness on the structural and optical properties of $Na_2WO_4$ films, XRD technique was employed to explore the structural modification improvement due to increasing the thickness, and EDX analysis method was used to reveal information about the composition of the films. UV technique has been employed to monitor the optical band gap variation with film thickness. Additionally, sensing abilities at room temperature (25 °C) have been investigated. To our knowledge, this is the first study on $Na_2WO_4$ films for sensing vapor gas of ethanol ($C_2H_5OH$), acetone ($C_3H_6O$) methanol ($CH_3OH$) and ammonia hydroxide ($NH_4OH$).

## 2. Experimental

$Na_2WO_4$ thin films were prepared on Si(100) and glass substrates using thermal evaporation technique. The residual pressure in the chamber was lower than $3.33 \times 10^{-3}$ Pa and the working pressure was about $2.39 \times 10^{-2}$ Pa. The substrates were heated to 400 °C. Sodium tungstate ($Na_2WO_4{\cdot}2H_2O$) (Merck) was used as a target to prepare the films. The thickness has been varied from 500 nm to 3000 nm. The quality of the films depended crucially on the deposition parameters.

The morphology and thickness of the films were observed by a scanning electron microscope (SEM) TESCAN Vega\\XMU (Czech Republic) operated at 30 kV, equipped with energy dispersive X-ray spectroscopy (EDX) system used for atomic composition determination of the $Na_2WO_4$ films. The XPS analysis was performed using SPECS UHV/XPS/AES spectrometer equipped with a monochromated AlKα X-ray radiation source (1486.6 eV) operating at 250 W and a fixed pass energy of 20 eV [23]. AFM (Park Scientific Instruments) AP-0100 model was used to explore the films morphology (the mean grain size, grain distribution and surface roughness). In addition, the structural properties of the films were characterized by X-ray diffraction (XRD) using STOE transmission X-ray diffractometer Stadi P (Germany) with $CuK_\alpha$ ($\lambda = 0.15405$ nm) radiation. The sensing studies were performed using a static gas chamber to sense gas vapors of methanol, ethanol, acetone, $H_2O$ and $NH_3$ gases in air ambient. The $Na_2WO_4$ films were used as sensing elements at room temperature (25 °C), where temperature was measured by a thermocouple. The method of concentration calculation was described in the previous work [6], where the electrical resistance of the sensing element was measured by a simple two-probe configuration, before and after exposure to vapor, using a Keithley 237 instrument for I-V characteristics measurement via a suitable feed-through. The sensitivity (S) of the sensing element is defined as:

$$Sensitivity(\%) = |(Rg - Ra)/Ra| \times 100 \qquad (1)$$

where Ra and Rg are values of resistance before and after exposure to gas vapor, respectively.

## 3. Results and discussion

### 3.1. SEM and AFM study

Fig. 1a shows the surface morphology of a film deposited on Si by thermal evaporation technique. The surface has nanocrystalline structure in a spherical form. Fig. 1b shows the cross-sectional view of this film. The structure looks dense and its thickness is about 3000 nm. The morphology of the films principally depends on the conditions of evaporation, spreading and precipitation rates and decomposition reaction. Abdallah et al. [6] obtained porous morphology using spray pyrolysis

technique which plays an important role in the adsorption of gas molecules and, in consequence, influences the sensing.

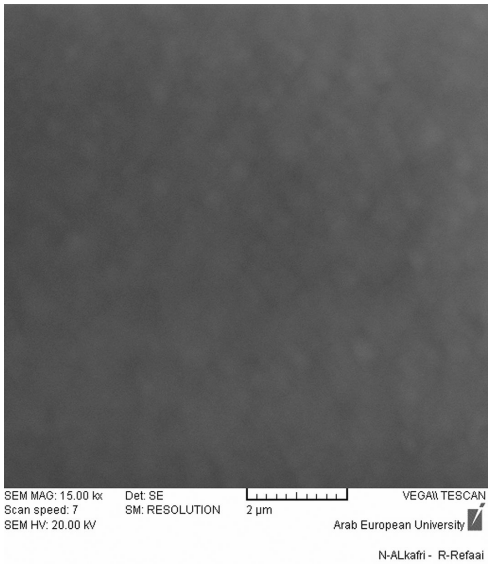


(a)

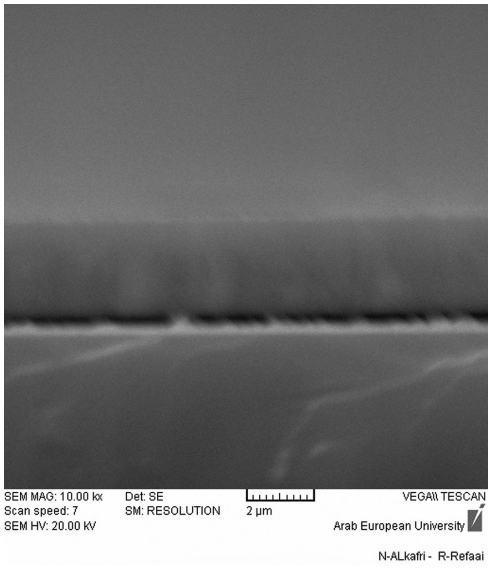


(b)

Fig. 1. SEM images (a) surface morphology; and (b) cross section of 3000 nm film.

Fig. 2 shows an AFM image of surface morphology of a $Na_2WO_4$ film. Fig. 2a displays a 3D image of 500 nm thick film and Fig. 2b is a 3D image of a film with 3000 nm thickness. The evolution of roughness $R_a$ (roughness average) and $R_q$ (root mean square roughness) has been obtained from AFM measurements and it slightly increased with the film thickness (Fig. 2a and Fig. 2b).

Fig. 2c shows a surface (2D) image and Fig. 2d corresponding roughness profile, where the number of grains is 472, roughness of $R_a$ is 4.7 nm and $R_q$ is 5.8 nm for the 3000 nm thick film. The morphology shows that the film prepared by thermal evaporation method is smooth and displays nanostructure features, while the film fabricated in the previous work [6] by spray pyrolysis displayed porous structure.

### 3.2. EDX and XPS study

The composition of the $Na_2WO_4$ film with 3000 nm thickness was examined by means of EDX analysis. X-ray peaks corresponding to Na, W and O elements present in the film are clearly shown in the EDX spectrum (Fig. 3).

Table 1. EDX composition for the film with 3000 nm thickness.

| Element | wt.% | at.% |
|---|---|---|
| O K | 21.05 | 49.96 |
| Na K | 23.33 | 38.55 |
| W M | 55.62 | 11.49 |

Chemical formula, $Na_2WO_4$, of the films prepared by evaporation method can be deduced from Table 1. XRD results, presented in the next section, confirm this.

X-ray photoelectron spectroscopy (XPS), was employed to obtain the chemical state of tungsten on the surface of the films. Fig. 4 presents the spectrum survey mode for $Na_2WO_4$ film with 500 nm thickness, where Na-ls peak is located at 1070 eV [24], W4-$d_{5/2}$ (246 eV), W4-$d_{3/2}$ (259 eV), W4-$p_{3/2}$ (422 eV) and W4-$p_{1/2}$ (492 eV). The peak located at approximately 975 eV corresponds to O KLL Auger.

Fig. 5a shows a peak at 29.7 eV related to the W metal element, while Narasimham et al. [25] found it at about 30.5 eV to 31.3 eV which is close to the obtained results. Also, the spectra present a symmetrical peak of W 4f incorporated with $WO_3$ (W $4f_{7/2}$(35.6 eV)) and (W $4f_{5/2}$(36.7 eV)). However, Kawasaki et al. [26] found the peak corresponding

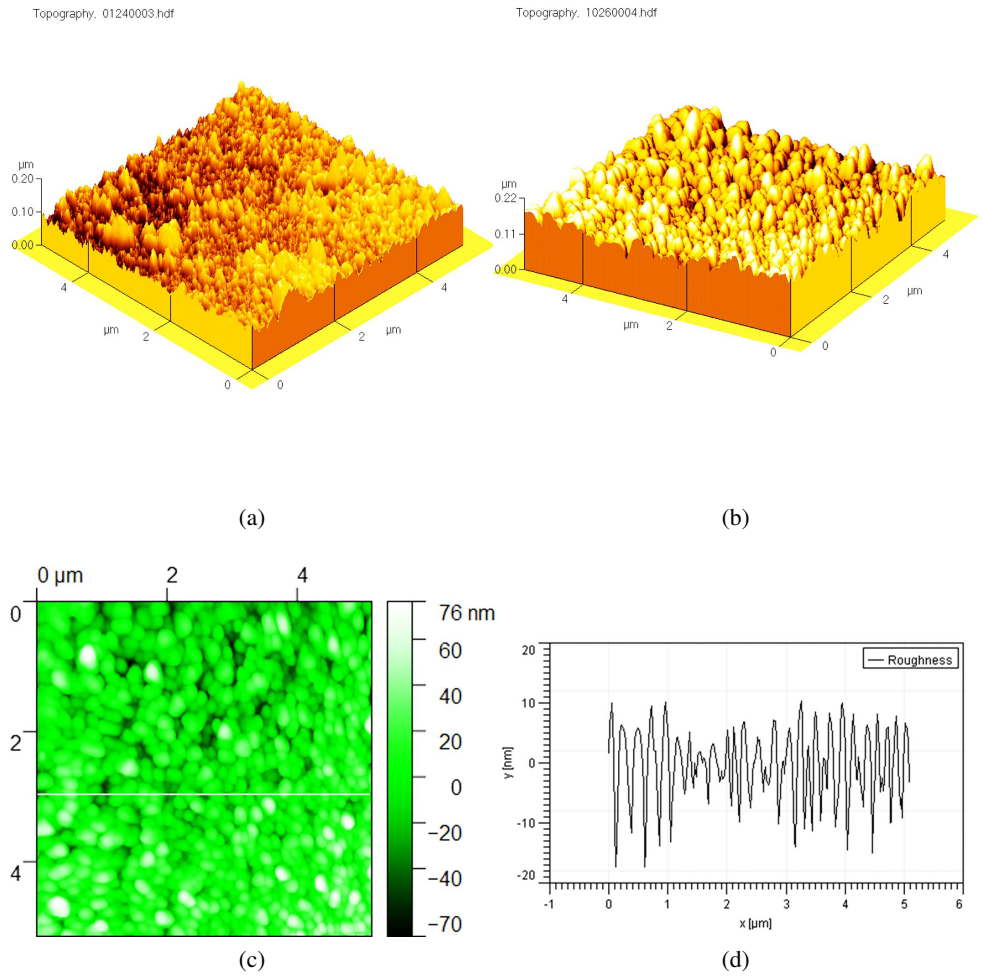


Fig. 2. AFM images of the films deposited on Si substrate (a) 3D image of 500 nm thick film, (b) 3D image of 3000 nm thick film, (c) surface image and (d) corresponding roughness profile of 3000 nm thick film.

to $WO_3$ at 37.9 eV ($W4f_{5/2}$) and 38.8 eV ($W4f_{7/2}$). Similarly, Bertus et al. [27] found the peaks at 37.9 eV ($W4f_{5/2}$) and 35.7 to 38.8 eV ($W4f_{7/2}$). Zhuiykov et al. [28] found the W 4f peaks of $WO_3$ for the deposited thin film between 36.2 eV to 35.2 eV. Table 2 summarizes the above results.

Fig. 5b shows the peak O 1s at 531.1 eV connected with $WO_x$ [26]. The O1s peak was deconvoluted into W=O (530.6 eV), OH-groups (531.4 eV) and water bound at the surface of the sample (533.2 eV). The Na 1s peak is located at 1071.40 eV (Fig. 5c), which is slightly larger than that of either NaOH powder (1071.26 eV) or sodium lactate (1071.30 eV) [29]. It has been observed that the peak position shifts to a higher binding energy (1071.89 eV) which is of 0.63 eV higher than the peak position of NaOH powder and of 0.59 eV higher than that of sodium lactate after 30 s of ion sputtering. This explains while a substantial portion of the sodium located at the film surface may originate from adsorbed ligand and/or sodium hydroxide and sodium existing primarily in a different chemical state within the bulk of the film.

No difference has been observed between prepared samples with other thicknesses, since the XPS probes the first thin layer (about 10 nm), as explained by Mrada et al. [23].

Table 2. XPS for peaks $W4f_{5/2}$ and $W4f_{7/2}$.

| | W4f incorporated with metal W | W4f ($WO_3$) [26] | W4f ($WO_3$) [27] | W4f ($WO_3$) [28] | This work W4f ($WO_3$) |
|---|---|---|---|---|---|
| $W4f_{5/2}$ | 33.8 eV | 37.9 eV | 37.9 eV | | 36.7 eV |
| $W4f_{7/2}$ | 31.7 eV | 38.8 eV | 35.7 eV | 36.2 eV – 35.2 eV | 35.6 eV |

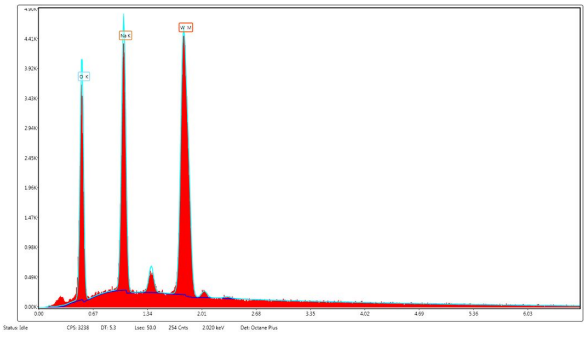

Fig. 3. EDX characterization of the film with 3000 nm thickness deposited on Si substrate.

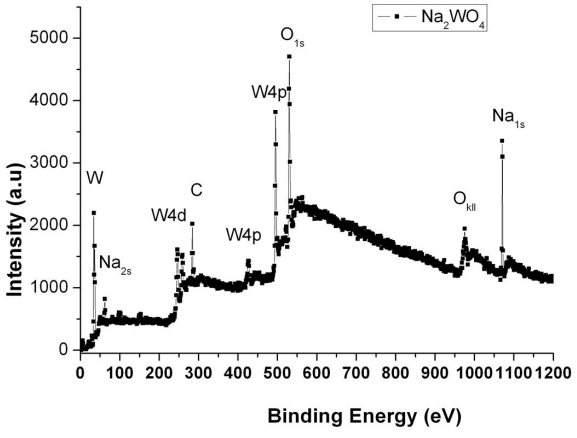


Fig. 4. XPS spectra survey for deposited film with 500 nm thickness.

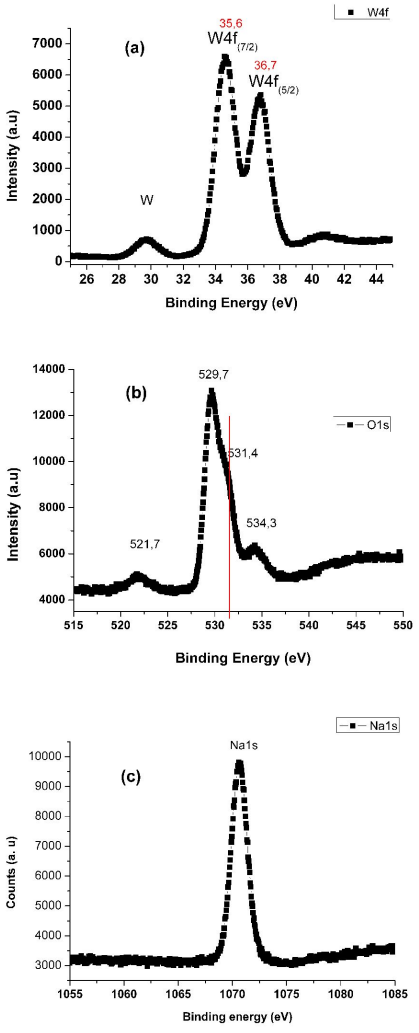


Fig. 5. High resolution XPS spectra for film with 500 nm thickness (a) for W4f, (b) for O1s-level and (c) for Na1s peak.

## 3.3. XRD study

XRD patterns of the deposited films with different thicknesses are shown in Fig. 6a. The diffraction peaks with (1 1 1), (2 2 0) and (3 1 1) orientations are located at 16.83°, 27.67°and 32.55°, respectively, and can be indexed to the cubic structure of $Na_2WO_4$ with the lattice parameter a = 0.91297 nm. This is in a good agreement with the JCPDS Card No. 12-772. These results are close to the previous ones [6], where $Na_2WO_4$ films were prepared by ultrasonic spray pyrolysis, using $Na_2WO_4 \cdot 2H_2O$ solution at 475 °C. Some groups [30] have reported cubic phase of $WO_3$ by

adding Li and H elements ($Li_xWO_3$, $H_xWO_3$). In this paper, the films characterized by XRD and by EDX confirm the formula $Na_2WO_4$ according to JCPDS Card No. 12-772 as well as EDX composition.

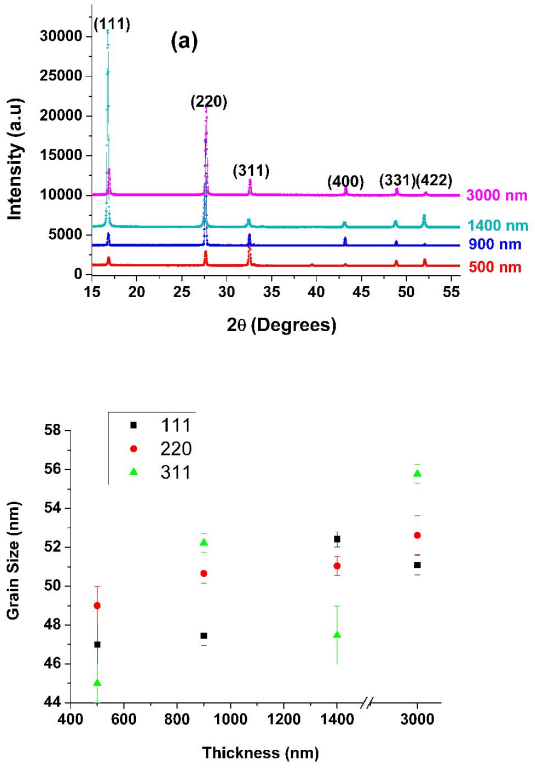


Fig. 6. (a) X-ray diffraction patterns for films deposited on Si substrate, (b) grain size evolution for the deposited films with different thicknesses.

The grain sizes of the crystallites were calculated using the Scherrer equation for (1 1 1), (2 2 0) and (3 1 1) peaks of $Na_2WO_4$ films and it was found that the crystallite size increases for the three orientations with increasing the film thickness (Fig. 6b). These results are consistent with the ones obtained by other groups [17]. In our previous work [6], the grain size also increased with increasing the thickness of $Na_2WO_4$ film prepared by ultrasonic spray pyrolysis and ZnO films prepared by RF magnetron sputtering. The structural properties are affected by many parameters, such as substrate temperature and film thickness (deposition time) [31].

## 3.4. Optical study

Fig. 7a shows the optical transmittance of $Na_2WO_4$ films with various thicknesses. The optical transmittance provides useful information about the optical band gap of semiconductor [31, 32]. It is observed that the average transmittance of the samples in the visible and near infrared range is varied with the thickness from 90 % to 78 %.

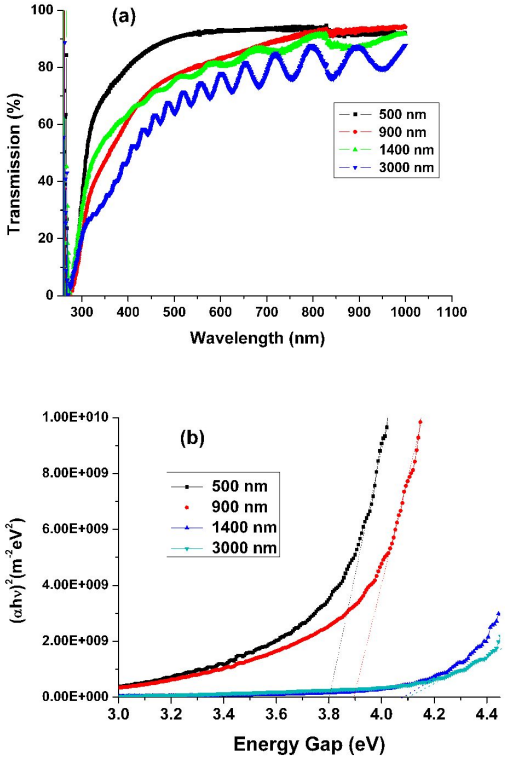


Fig. 7. (a) Optical transmittance spectra for $Na_2WO_4$ films on glass substrates, (b) the band gap of the films with different thickness.

The optical band gap of the $Na_2WO_4$ films is varying from 3.8 eV to 4.1 eV. It is well known that the optical band gap of $WO_3$ is affected by defects as well as the grain size [33, 34]. In our case, we found a connection between better quality and bigger gap. In the previous work, the gap and the quality revealed the same behavior for ZnO film [35] and for $SnO_2$ film [36]. These results are in contrast with the work by Rao et al. [37] and Abdallah [38] where the energy gap was inversely proportional to the crystallite size.

### 3.5. Sensitivity study

The relationship between the films sensitivity and ethanol vapor concentration at 25 °C is shown in Fig. 8a. The sensitivity increases quasi- linearly with ethanol vapor concentration (Fig. 8a). This evolution may be attributed to the availability of sufficient number of sensing sites interacting with the ethanol vapor as demonstrated by Khadayate et al. [39]. However, they found the higher sensitivity at 400 °C (75 ppm concentration) and explained that both temperature and concentration influence sensitivity. It is also consistent with the results of Chang et al. [40] where the response to gases (ethanol or acetone) of ZnO increased with their concentration.

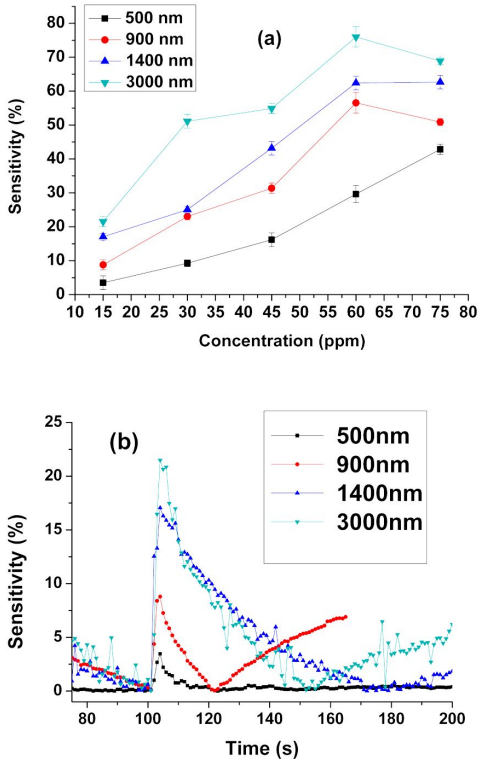


Fig. 8. (a) Dependence of sensitivity on ethanol vapor concentration for $Na_2WO_4$ films with different thicknesses; (b) relationship between film thickness and sensitivity of films deposited at several deposition time (corresponding to different thicknesses from 500 nm to 3000 nm) for 15 ppm ethanol vapor in air.

Fig. 8b presents the sensitivity evolution with thicknesses (500 nm to 3000 nm) for ethanol vapor concentration (15 ppm to 75 ppm). The increase of ethanol vapor concentration results in an increase in sensitivity response; this behavior was also observed by Kanda et al. [17], where the sensitivity increased with an increase of both the thickness and mean grain size .

Fig. 8b shows that thicker $Na_2WO_4$ films have a response time ∼5 s and recovery time ∼145 s for 15 ppm ethanol vapor. These results are better than the results obtained by Khadayate et al. [39] who carried theirs studies at 400 °C. However, in another study on ZnO and Sn-ZnO films (CBD), the average response time was about 55 s [40]. In work [31], when the thickness increased, the crystalline quality of ZnO film improved [31], and higher response to ethanol gases at 350 °C was obtained. Ahmad et al. [16] conducted studies on ethanol sensing properties of $WO_3$ nanorods at 400 °C, thus, one can conclude, that the response time is short, and could be attributed to the adsorption-desorption type of sensing mechanism [41]. It is known that oxygen is adsorbed on ZnO surface as $O^-$ or $O^{2-}$ by capturing electrons [41] so similar mechanism may act in $Na_2WO_4$ film. The response/recovery time is an important parameter, used for characterizing sensors. It is defined as the time required to reach 90 % of the final change in voltage or resistance, when the gas is turned on or off, respectively.

Fig. 9 shows the sensitivity of $Na_2WO_4$ films with different thicknesses to different gasses, namely ethanol ($C_2H_5OH$), acetone ($C_3H_6O$), methanol ($CH_3OH$), and ammonia hydroxide ($NH_4OH$) vapor at 20 ppm concentration.

Our $Na_2WO_4$ films exhibit minimum sensing properties for acetone ($C_3H_6O$), whereas, Wongchoosuk et al. [42] found a strong response to ethanol for ZnO in comparison to acetone, toluene, propan-2-ol and acetonitrile, using thermal oxidation technique without ZnO doping.

Fig. 9 shows the highest sensitivity for 20 ppm ammonia hydroxide ($NH_4OH$) vapor at room temperature. This result is close to the one obtained by Dighavkar et al. [43] who obtained the highest selectivity for $NH_3$ in comparison to all other tested

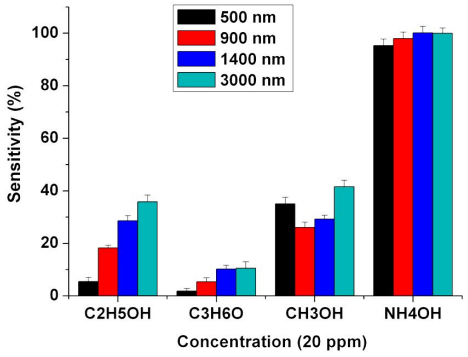


Fig. 9. Sensitivity of $Na_2WO_4$ films with different thicknesses to different gases: ethanol ($C_2H_5OH$), acetone ($C_3H_6O$) methanol ($CH_3OH$) and ammonia hydroxide ($NH_4OH$) vapor at 20 ppm concentration.

gases viz: $NO_2$, LPG, ethanol vapors, $CO_2$and $H_2S$, for ZnO nanopowders synthesized using chemical bath deposition (CBD) method. $NH_3$ is a reducing gas, and it reacts with oxygen ions on the surface of the film. Reduction on the film surface increases the number of free carriers. Therefore, resistance of the film decreases with reducing gases [44]. The response to humidity ($H_2O$) and ethanol ($C_2H_5OH$) is higher than to methanol ($CH_3OH$), acetone ($C_3H_6O$) and ammonia ($NH_4^+$) gases. The sensitivity decreases as the hydrogen bond energy (polarization) decreases gradually for $H_2O$, $C_2H_5OH$, $CH_3OH$, $C_3H_6O$ and $NH_4$. Normally, the larger the energy, the stronger the gas adsorption so the adsorption energy of $H_2O$ on the Zn doped $SnO_2$ films is relatively higher than on the others [36]. This is consistent with Wang et al. [45] who investigated the adsorption mechanism of $H_2$ on Cu-doped $SnO_2$ surface.

## 4. Conclusions

Thermal evaporation technique was used to prepare $Na_2WO_4$ films with various thicknesses on silicon and glass substrates. Physical properties and composition of the prepared films were investigated. The crystallite size was found to increase with increasing film thickness. SEM and AFM were used to monitor morphology of the films and composition of the film has been verified by EDX and XPS techniques. The optical band gap of the $Na_2WO_4$ films varied from 3.8 eV to 4.1 eV. Ethanol vapor sensing properties were investigated at temperature of 25 °C for different gas concentrations. The thickest $Na_2WO_4$ film exhibited good ethanol vapor sensing properties with maximum sensitivity and a fast response time. In addition, the sensing properties of prepared films were studied for different vapors (ethanol, acetone ($C_3H_6O$) methanol ($CH_3OH$) and ammonia hydroxide ($NH_4OH$) at room temperature.

## Acknowledgements

Authors would like to thank Prof. I. Othman, the Director General of the AECS, for support, Dr. S. Rihawy and Dr. A.K. Jazmati for valuable discussion and Dr. W. Khouri for XRD measurements.

## References

[1] SANTATO C., ULMANN M., AUGUSTYNSKI J., *J. Phys. Chem. B*, 5 (2001), 936.
[2] RS C., BW F., *Phys. Rev. Lett*, 39 (1977), 232.
[3] DICKENS P.G., WHITTINGHAM M.S., *Q. Rev. Chem. Soc.*, 1 (1968), 30.
[4] GOODENOUGH J.B., *Prog. Solid. Sate Ch.*, 5 (1971), 145.
[5] CLARKE R., *Phys. Rev. Lett.*, 39 (1977), 1550.
[6] ABDALLAH B., KAKHIA M., SHAKER S.A., *Comp. Interfaces*, 23 (2016), 663.
[7] DAKHEL A.A., *Mater. Res. Innov.*, 1 (2017), 55.
[8] SUN H.-T., CANTALINI C., LOZZI L., PASSACANTANDO M., SANTUCCI S., PELINO M., *Thin Solid Films*, 1 (1996), 258.
[9] CLIFFORD P.K., TUMA D.T., *Sensor. Actuat.*, 3 (1982), 255.
[10] YU-DE W., ZHAN-XIAN C., YAN-FENG L., ZHEN-LAI Z., XING-HUI W., *Solid. State. Electron.*, 5 (2001), 639.
[11] ITO K., OHGAMI T., NAKAZAWA T., *Sensor. Actuat. B Chem.*, 3 (1993), 161.
[12] ANDO M., SUTO S., SUZUKI T., TSUCHIDA T., NAKAYAMA C., MIURA N., YAMAZOE N., *Chem. Lett.*, 2 (1994), 335.
[13] CHIU H.C., TSEUNG A.C.C., *Electrode. Electrochem. Solid State Lett.*, 2(10) (1999), 540.
[14] QU W., WLODARSKI W., *Sensor. Actuat. B Chem.*, 1 – 3 (2000), 4.
[15] NAJDOSKI M.Z., TODOROVSKI T., *Mater. Chem. Phys.*, 2 – 3 (2007), 483.
[16] AHMAD M.Z., KANG J.H., SADEK A.Z., MOAFI A., SBERVEGLIERI G., WLODARSKI W., *Procedia Engineering*, 47 (2012), 358.
[17] KANDA K., MAEKAWA T., *Sensor. Actuat. B Chem.*, 108 (2005), 97.

[18] PATIL P.S., *B. Mater. Sci.*, 4 (2000), 309.
[19] MOHAMMAD AL A., GILLET M., *Thin Solid Films*, 1 – 2 (2002), 302.
[20] PONZONI A., COMINI E., FERRONI M., SBERVEGLIERI G., *Thin Solid Films*, 1 (2005), 81.
[21] PATEL K., PANCHAL C., KHERAJ V., DESAI M., *Mater. Chem. Phys.*, 1 (2009), 475.
[22] ZHU Y.Q., HU W., HSU W.K., TERRONES M., GROBERT N., HARE J.P., KROTO H.W., WALTON D.R.M., TERRONES H., *Chem. Phys. Lett.*, 5 – 6 (1999), 327.
[23] MRADA O., ISMAILA I.M., ABDALLAHB B., RIHAWYA M.S., *J. Optoelectron. Adv. Mat.*, 9 – 10 (2014), 1099
[24] KISHI K., KIRIMURA H., FUJIMOTO Y., *Surf. Sci.*, 3 (1987), 586.
[25] NARASIMHAM A.J., GREEN A., MATYI R.J., KHARE P., VO T., DIEBOLD A., LABELLA V.P., *AIP. Adv*., 11 (2015), 117107.
[26] KAWASAKI H., MATSUNAGA T., GUAN W., OHSHIMA T., YAGYU Y., SUDA Y., *J. Plasma Fusion Res*., 8 (2009), 1431.
[27] BERTUS L.M., FAURE C., DANINE A., LABRUGERE C., CAMPET G., ROUGIER A., DUTA A., *Mater. Chem. Phys.*, 1 (2013), 49.
[28] ZHUIYKOV S., HAI Z., XU H., XUE C., *Int. J. Mater. Metall. Eng.*, 1 (2017), 46.
[29] ZHU C., OSHEROV A., PANZER M.J., *Electrochim. Acta*, 30 (2013), 771.
[30] REGRAGUI M., ADDOU M., OUTZOURHIT A., IDRISSI EL E., KACHOUANE A., BOUGRINE A., *Sol. Energ. Mat. Sol. C.*, 4 (2003), 341.
[31] AL-KHAWAJA S., ABDALLAH B., SHAKER S.A., KAKHIA M., *Comp. Interface.*, 3 (2015), 221.
[32] ABDALLAH B., JAZMATIA A.K., REFAAI R., *Mat. Res.*, 3 (2017), 607.
[33] PRATHAP P., REVATHI N., SUBBAIAH Y.P.V., REDDY K.T.R., *Phys.-Condens. Mat.*, 3 (2008), 035205.
[34] WANG J., GAO L., *J. Mater. Chem.*, 10 (2003), 2551.
[35] RAHMANE S., DJOUADI M.A., AIDA M.S., BARREAU N., ABDALLAH B., ZOUBIR H.N., *Thin Solid Films*, 1 (2010), 5.
[36] ABDALLAH B., JAZMATI A.K., KAKHIA M., *Optik*, 158 (2018), 1113.
[37] RAO K.S., KANTH B.R., DEVI G.S., MUKHOPADHYAY P., *J. Mater. Sci.-Mater. El,* 9 (2011), 1466.
[38] ABDALLAH B., NASRALLAH F., ALNAMA K., *Mod. Phy. Lett. B*, 04 (2019),
[39] KHADAYATE R.S., WAGHULDE R.B., WANKHEDE M.G., SALI J.V., PATIL P.P., *B. Mater. Sci.,* 2 (2007), 129.
[40] LI X., CHANG Y., LONG Y., *Mater. Sci. Eng. C*, 4 (2012), 817.
[41] LUPAN O., URSAKI V.V., CHAI G., CHOW L., EMELCHENKO G.A., TIGINYANU I.M., GRUZINTSEV A.N., REDKIN A.N., *Sensor. Actuat. B Chem.*, 1 (2010), 56.
[42] WONGCHOOSUK C., CHOOPUN S., TUANTRANONT A., KERDCHAROEN T., *Mat. Res Innov.*, 13 (2009), 185.
[43] DIGHAVKAR C., *Arch. Appl. Sci. Res*, 6 (2013), 96.
[44] LU J. G., CHANG P., FAN Z., *Mater. Sci. Eng. R Rep.*, 1 – 3 (2006), 49.
[45] WANG F., FAN J., SUN Q., JIANG Q., CHEN S., ZHOU W., *J. Nanomater*, (2016), 1.

*Received 2018-10-11*
*Accepted 2019-04-23*